$He^3(\alpha,\gamma)Be^7$ Reaction*

P. D. PARKER AND R. W. KAVANAGH
California Institute of Technology, Pasadena, California
(Received 8 May 1963)

The $He^3(\alpha,\gamma)Be^7$ reaction has been investigated using gaseous helium targets behind thin nickel foils and using monoenergetic alpha-particle beams with energies from 0.42 to 5.80 MeV. The prompt gamma rays were detected using NaI(Tl) scintillation spectrometers, and the resulting pulse-height spectra were analyzed to determine both the total capture cross section and the branching ratio between the cascade and the crossover transitions as functions of energy. These cross-section measurements have been used to obtain a new value for the zero-energy intercept of the cross-section factor $S(E)$ for this reaction: $S_0=0.47\pm0.05$ keV-b, and $(dS/dE)_0=-2.8\times10^{-4}$ b.

INTRODUCTION

THE direct-capture reaction $He^3(\alpha,\gamma)Be^7$ is a particularly interesting member of the class of direct-capture reactions because of the large energy range ($0.0\leq E_\alpha\leq6.8$ MeV) over which it is nonresonant and because of the extensive information that is available from elastic-scattering investigations[1–3] about the phase shifts for the various partial waves necessary to describe the initial-state wave function. A detailed discussion of the use of these phase shifts in the calculation of theoretical cross sections and angular distributions for such direct-capture reactions is presented in the paper immediately following this one.[4]

Furthermore, the $He^3(\alpha,\gamma)Be^7$ reaction is of interest in nuclear astrophysics since it serves as a He^3-burning reaction for the termination of the proton-proton chain. In the proton-proton chain, once He^3 has been produced via the reactions

$$H^1(p,\beta^+\nu)D^2(p,\gamma)He^3,$$

the chain is normally terminated by converting the He^3 into He^4 through one of the two following He^3-burning reactions:

$$He^3(He^3,2p)He^4 \quad (1)$$

$$He^3(\alpha,\gamma)Be^7(e^-,\nu)Li^7(p,\alpha)He^4 \quad (2a)$$

$$He^3(\alpha,\gamma)Be^7(p,\gamma)B^8(\beta^+\nu)Be^{8*}(\alpha)He^4. \quad (2b)$$

Hence, the terminations via the $He^3(\alpha,\gamma)Be^7$ reaction produce one He^4 for every $H^1(p,\beta^+\nu)D^2$ reaction, compared to the yield of only one He^4 for every two $H^1(p,\beta^+\nu)D^2$ reactions through the $He^3(He^3,2p)He^4$ termination. Therefore, since the rate of the proton-proton chain is governed by the $H^1(p,\beta^+\nu)D^2$ reaction, completion of the chain via the $He^3(\alpha,\gamma)Be^7$ reaction instead of the $He^3(He^3,2p)He^4$ reaction doubles the rate of He^4 production and nearly doubles the rate of energy generation [a factor of 1.95 for the Li^7 branch (2a) and a factor of 1.46 for the B^8 branch (2b) due to energy losses in the form of neutrinos].[5,6] This difference in the efficiencies of these two terminations makes a knowledge of the relative importance of these reactions essential to the study and generation of models of stellar interiors for stars operating on the proton-proton chain.

Previous measurements on the $He^3(\alpha,\gamma)Be^7$ reaction and the mirror reaction $H^3(\alpha,\gamma)Li^7$ have been reported by Holmgren and Johnston.[7] However, recent work by Griffiths[8] is in marked disagreement with the total cross-section measurements of Holmgren and Johnston for the $H^3(\alpha,\gamma)Li^7$ reaction. The present experiment has been carried out to extend the cross-section measurements for the $He^3(\alpha,\gamma)Be^7$ reaction in order to check the predictions of the direct-capture theory and to redetermine the role of this reaction in astrophysics.

PROCEDURE

Figure 1 indicates the construction of the gas target system used in this experiment. The monoenergetic incident beam was obtained by magnetic analysis from the Kellogg Radiation Laboratory 3-MV electrostatic accelerator and from the 6-MV ONR-CIT tandem accelerator. Alpha-particle beams were used instead of He^3, in spite of the resultant increases in energy losses, because of the large reduction in gamma-ray background

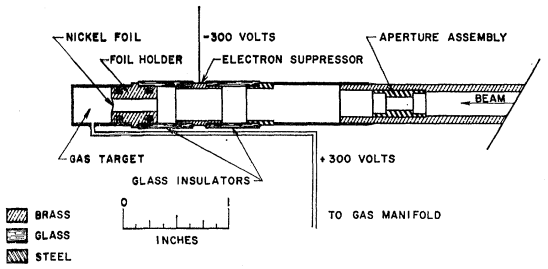

FIG. 1. Scale drawing of the gas-target assembly.

* Supported by the U. S. Office of Naval Research.

[1] P. D. Miller and G. C. Phillips, Phys. Rev. **112**, 2048 (1958).
[2] C. M. Jones, A. C. L. Barnard, and G. C. Phillips, Bull. Am. Phys. Soc. **7**, 119 (1962).
[3] T. A. Tombrello and P. D. Parker, Phys. Rev. **130**, 1112 (1963).
[4] T. A. Tombrello and P. D. Parker, following article, Phys. Rev. **131**, 2582 (1963).
[5] W. A. Fowler, Astrophys. J. **127**, 551 (1958).
[6] W. A. Fowler, Mem. Soc. Roy. Sci. Liege **3**, 207 (1960).
[7] H. D. Holmgren and R. L. Johnston, Phys. Rev. **113**, 1556 (1959).
[8] G. M. Griffiths, R. A. Morrow, P. J. Riley, and J. B. Warren, Can. J. Phys. **39**, 1397 (1961).

that it was thereby possible to achieve. The target gas was contained in the small gas cell (approximately 1 cm in length and 1 cm in diameter) and was separated from the high-vacuum beam tube by a thin nickel foil, typically 6250 Å thick.[9] At beam energies below 1.5 MeV, this was replaced by a 5000-Å nickel foil on which 1000 to 2000 Å of copper had been evaporated to improve the thermal conductivity; in this way we were able to use beams of at least 0.4 μA over the entire energy range of this experiment. The target gas could be switched rapidly between He^3 and He^4, the latter being used for background runs. This alternation was carried out from four to ten times during a series of runs at each energy in order to average out small background variations.

The target thickness was determined from a measurement of the length of the gas cell and measurements of the temperature and pressure in the gas cell. The pressure was measured using either a mercury manometer or a bourdon gauge which was calibrated with a mercury manometer; target pressures varied from 100 to 494 mm. In the determination of the target temperature, local heating by the incident beam was taken into account by measuring the change in the effective thickness of the gas target as a function of the incident beam intensity. This was accomplished by using a thick B^{10} target in the back of the target chamber and observing the shift of the position of the 1.518-MeV resonance in $B^{10}(\alpha,p)C^{13}$ as a function of the incident beam intensity. These measurements indicated an effective target temperature of 345°K at a beam current of 0.45 μA. Simple conductivity calculations suggest that most of this heating is due to energy losses in the entrance foil and the resultant heating of the gas near the foil.

Cylindrical 3-in.×3-in. NaI(Tl) scintillators were used to detect the gamma radiation. The resulting pulses were fed through conventional electronics and stored in a multichannel pulse-height analyzer. The various target-crystal geometries are shown in Fig. 2. The poor geometry (with the crystal face typically only $\frac{3}{8}$ of an inch from the center of the target) was dictated by the small cross sections involved and unfortunately prevented the observation of any angular anisotropy of the radiation that was smaller than about 25%. No anisotropies of this magnitude were observed, and the data were analyzed under the assumption that the radiation was isotropic. The maximum predicted anisotropies[4] in the region of this experiment are only of the order of 7%, and hence, are well below what we could have observed. Furthermore, any change in the crystal-target geometry to improve our angular resolution to allow us to see this effect would drastically reduce the counting rate, while the anisotropy is already smaller than the relative uncertainties in the points of this experiment.

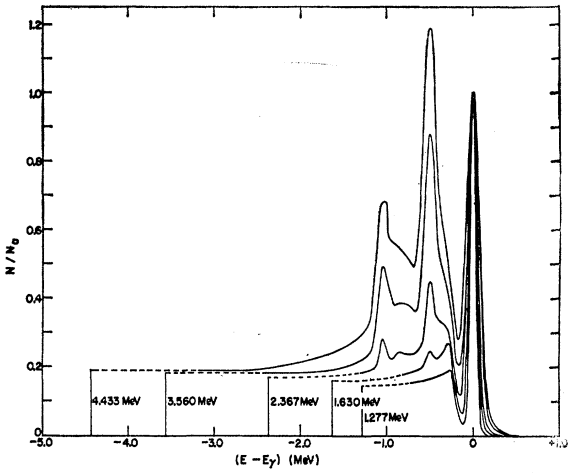

FIG. 3. The line-shape response calibration of the solid 3-in.×3-in. NaI(Tl) crystal as measured experimentally using various nuclear reactions to produce the monoenergetic gamma rays. The gamma-ray energy is indicated at the low-energy end of each function. From such a calibration, it is possible to interpolate the line-shape response at any intermediate energy.

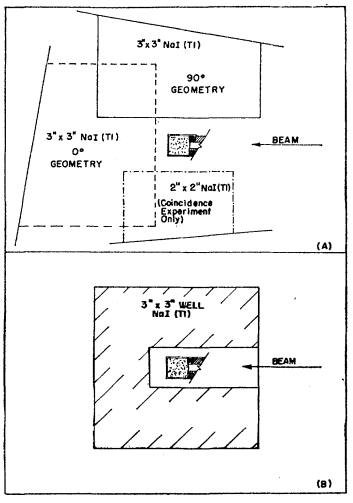

FIG. 2. The target-detector geometry for the various NaI(Tl) crystals used. (A) The configurations employed with the solid cylindrical crystals, including the coincidence experiment. (B) The arrangement used with the 3-in.×3-in. crystal with a $\frac{3}{4}$-in.×2-in. well.

For each of the NaI(Tl) crystals, the total effective efficiency was calculated for these geometries using the tables of Grodstein[10] and taking into account the absorption of the materials between the crystal and the target gas. Further, the crystals were calibrated with respect to their line-shape response by using various monoenergetic gamma rays in the energy range $0.432 \leq E_\gamma \leq 4.433$ MeV. These measured response functions were then plotted as functions of $(E-E_\gamma)$, as suggested by Okano,[11] in order to simplify the interpolation used to determine these functions at intermediate energies. Such a plot is shown in Fig. 3. The photofraction (i.e., the fraction of the total gamma-ray spectrum located in the full-energy peak) of each of the crystals was then measured experimentally by observing these monoenergetic gamma rays using unshielded crystals

[9] Obtained from Chromium Corporation, Waterbury, Connecticut.

[10] G. W. Grodstein, Natl. Bur. Std. (U. S.), Circ. **583** (1957).
[11] K. Okano, J. Phys. Soc. Japan **15**, 28 (1960).

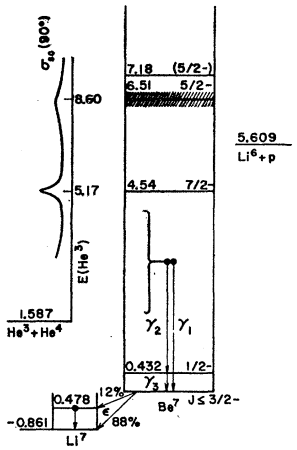

FIG. 4. Level diagram for Be^7 indicating the two possible gamma transitions in the region of this experiment as well as the various Q values involved and the locations and quantum numbers of the various excited states.

and the zero-intercept method of Zerby and Moran.[12] The photofraction was then combined with the total effective efficiency to yield the effective photoefficiency.

After applying dead-time corrections for the multichannel analyzer and total-time corrections for time-dependent background, the resulting spectra were analyzed by subtracting the He^4 spectrum from the He^3 spectrum to obtain the net $He^3(\alpha,\gamma)Be^7$ gamma-ray spectrum. The net spectrum was then analyzed on a computer to extract the various gamma-ray contributions, using the line-shape calibration of the scintillators. The Be^7 level diagram in Fig. 4 indicates that in the region investigated in this experiment there are two possible gamma-ray transitions, the crossover transition going directly to the ground state and the cascade transition proceeding through the 432-keV first excited state. Once the contributions of these transitions had been sorted out by obtaining a least-squares fit to the net experimental spectrum using the appropriate line-shape responses, an application of the effective photoefficiency yields immediately the number of each of the gamma rays produced in the target. A combination of this with the target thickness, as measured above, and with the number of incident alpha particles, as measured with a current integrator, yields the cross section for producing such gamma rays. A graphical example of the data reduction and least-squares unfolding of the experimental spectra is shown in Fig. 5 for the case where $E_{c.m.}=1248$ keV and $E_{\gamma_1}=2890$ keV with the 3-in.×3-in. crystal at 0° to the incident beam.

From such an analysis, it is then possible to obtain independent values for the cross sections of both transitions. The data can then either be presented in terms of these two cross sections or be expressed in terms of independent values for the total cross section and the branching ratio. The latter set of parameters proved more suitable because for almost half of the cases it was impractical to carry out such a least-squares analysis of the net spectrum. Such cases occur, for example, at beam energies below 1.0 MeV because of the low counting rates and resulting poor statistics, and above 3.5 MeV because of the alteration of the line-shape response of the crystals by absorbers placed between the crystals and the target to reduce the intensity of low-energy radiation from such sources as Coulomb excitation in the platinum beam stopper. For these cases it was possible to extract only one independent number, and, since the branching ratio remained essentially constant over the entire range of this experiment, the total cross section was the logical parameter to present for such data.

Since the target gas was located behind a foil that was 250 to 550 keV thick to the incident alpha particles, the center-of-mass energies at which these measurements were made were determined either by actually measuring the thicknesses of the entrance foils using the 1.518-MeV resonance in $B^{10}(\alpha,p)C^{13}$ or by using the fact that for capture reactions the energy of the prompt gamma radiation (allowing for Doppler shifting) is just the sum of the center-of-mass energy and the Q value for the reaction. In the cases where both of these methods were used, the agreement between the two was within the experimental error.

RESULTS

The experimental results are presented in Figs. 6–8. Figure 6 is a plot of the total capture cross section as a function of the center-of-mass energy. As a check on the unfolding techniques described above, a coincidence measurement was made to obtain an independent value for the cross section for the cascade transition by using

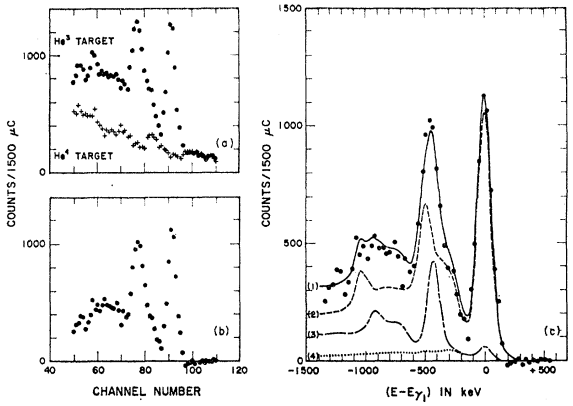

FIG. 5. Graphical representation of the data reduction and analysis for the case of $E_{c.m.}=1248$ keV. (a) The dots represent the raw NaI(Tl) spectrum obtained using He^3 as the target gas while the crosses represent the raw spectrum obtained under identical conditions using He^4 gas in the target chamber. (b) The dots represent the net $He^3(\alpha,\gamma)Be^7$ gamma-ray spectrum obtained by subtracting the He^4 spectrum from the He^3 spectrum in (a). (c) The net experimental $He^3(\alpha,\gamma)Be^7$ spectrum is represented by the dots. Curve (1) is the least-squares fit to the net spectrum obtained by varying the normalizations of curves (2) and (3), where (2) is the response function for the crossover transition and (3) is the response function for the cascade transition including the effects of coincident summing. Curve (4) is just the contribution of such summing to the cascade response function.

[12] G. D. Zerby and H. S. Moran, Nucl. Instr. Methods 14, 115 (1961).

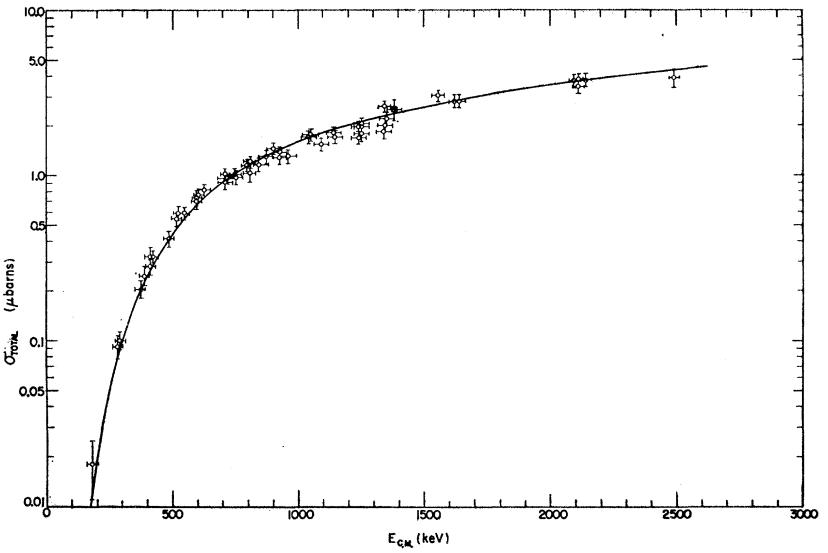

FIG. 6. The total capture cross section as a function of the center-of-mass energy. The circles are the experimental measurements, and the solid curve is the prediction of the theory in Ref. 4. The solid square at $E_{c.m.}=1378$ keV is the coincidence measurement.

two NaI(Tl) scintillators and requiring a coincidence between the two members of the cascade transition. The cross section derived in this way agreed well with the cascade cross sections obtained by the unfolding process. Converted to a total cross section by using the measured branching ratio, the coincidence point is shown in Fig. 6 as the solid square at $E_{c.m.}=1378$ keV. Figure 7 is a plot of the branching ratio (ρ), defined as the ratio of the cascade cross section to the cross section for the crossover transition. The data are consistent with a constant value for ρ over this region, and a statistical analysis indicates that $(73\pm3)\%$ of the transitions go directly to the ground state while the remaining $(27\pm3)\%$ cascade through the first excited state. The error bars in Figs. 6 and 7 (typically $\pm10\%$) are the total errors of the individual points and include such things as counting statistics, and uncertainties in the crystal efficiencies, the target thickness and the beam integration.

The solid curves in Figs. 6 and 7 are the predictions for the total capture cross section and the branching ratio based on the theory described in detail in the following paper.[4] It is sufficient to emphasize here that the agreement obtained between the theory and the experiment was achieved with the use of only two energy-independent parameters, the reduced widths of the two final states. Hence, only the normalization of these curves is subject to fitting, the curvature being completely defined by the independent elastic scattering experiments.

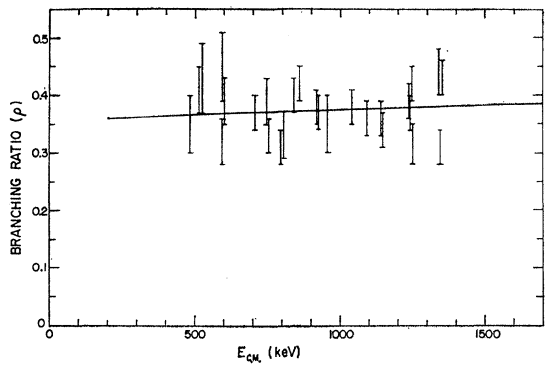

FIG. 7. The branching ratio (ρ) as a function of the center-of-mass energy, where $\rho\equiv\sigma(\text{cascade})/\sigma(\text{crossover})$. As in Fig. 6, the bars are the experimental values and the solid curve is from Ref. 4.

Finally, in order to apply our results to an analysis of the termination of the proton-proton chain we must extrapolate from our measurements to obtain cross sections at center-of-mass energies of the order of 10 to 20 keV. Such an extrapolation is most easily accomplished by first removing the penetration factor from the cross section and then working with the more nearly energy-independent "S factor,"[13]

$$S(E_{c.m.})=\sigma(E_{c.m.})E_{c.m.}\exp(31.28Z_0Z_1A^{1/2}/E_{c.m.}^{1/2})$$
$$=\sigma(E_{c.m.})E_{c.m.}\exp(163.78/E_{c.m.}^{1/2})\ \text{keV-b}.$$

This function is shown in Fig. 8 where the error bars and the solid curve represent the conversion of the measured cross sections and the theoretical prediction, respectively, and consequently this figure contains exactly the same information as Fig. 6, except that the dependence on the Coulomb barrier has been removed.

The shape of the theoretical curve having been defined by the elastic scattering experiments, the normalization of the curve shown here has been determined as the best fit to all of the experimental points. As such we are able to use the direct-capture theory together with the experimental points to obtain intercept parameters for $S(E)$ of

$$S_0=0.47\pm0.05\ \text{keV-b},$$
$$(dS/dE)_0=-2.8\times10^{-4}\,\text{b},$$

[13] E. M. Burbidge, G. R. Burbidge, W. A. Fowler, and F. Hoyle, Rev. Mod. Phys. **29**, 547 (1957).

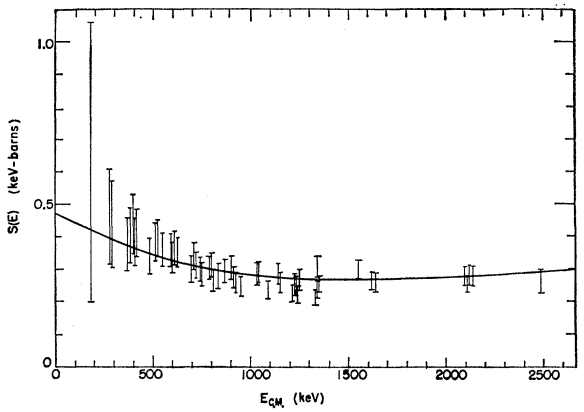

FIG. 8. The cross-section factor $S(E)$ as a function of the center-of-mass energy. The bars and solid curve are again the experimental values and the prediction of Ref. 4, respectively. At the intercept, $S_0=0.47\pm0.05$ keV-b, and $(dS/dE)_0=-2.8\times10^{-4}$ b.

which are considerably more accurate than our lowest energy points.

There may be some question as to whether the normalization for extrapolation purposes should not have been made to just the low-energy measurements. If such a normalization is made using only the data for $E_{c.m.}\leq625$ keV, one obtains an intercept of $S_0=0.51\pm0.07$ keV-b.

A combination of the S-factor intercepts of the other proton-proton-chain reactions with this new value for the $He^3(\alpha,\gamma)Be^7$ reaction allows us to determine the importance of each of the He^3-burning reactions as terminations for the proton-proton chain. A detailed discussion of the termination of this chain will be published elsewhere[14]; it is sufficient to note here that the new intercept is appreciably smaller than the value of 1.2 keV-b previously published by Holmgren and Johnston,[7] and consequently that in the temperature range below 16×10^6°K this new value reduces the importance ascribed in Refs. 5 and 6 to $He^3(\alpha,\gamma)Be^7$ as a He^3-burning reaction in stars like the sun.

ACKNOWLEDGMENTS

We are happy to acknowledge the assistance of the staff of the Kellogg Radiation Laboratory in carrying out this experiment. In particular, we are grateful to Professor William A. Fowler and Dr. T. A. Tombrello for their stimulus and helpful discussions.

[14] P. D. Parker, J. N. Bahcall, and W. A. Fowler, Astrophys. J. (to be published).

PHYSICAL REVIEW VOLUME 131, NUMBER 6 15 SEPTEMBER 1963

Direct-Capture Model for the $He^3(\alpha,\gamma)Be^7$ and $T(\alpha,\gamma)Li^7$ Reactions*

T. A. TOMBRELLO† AND P. D. PARKER
California Institute of Technology, Pasadena, California
(Received 8 May 1963)

Using the He^3+He^4 scattering phase shifts, the cross section for the $He^3(\alpha,\gamma)Be^7$ reaction is calculated on the basis of a He^3+He^4 model for the ground state and first excited state of Be^7. Capture of particles from the S, P, D, and F partial waves by means of $E1$, $M1$, and $E2$ transitions is considered. The results are in excellent agreement with the experimental data presented in the preceding paper and indicate that the reaction proceeds chiefly by means of $E1$ capture from the S and D waves. It is a surprising consequence that the D wave contributes an appreciable fraction of the total capture cross section for alpha-particle energies as low as 1 MeV. Using the same values for the reduced widths of the final states that were determined for the $He^3(\alpha,\gamma)Be^7$ reaction, similar calculations have also yielded excellent agreement with the experimental data for both the branching ratio and the total cross section of the mirror reaction $T(\alpha,\gamma)Li^7$.

INTRODUCTION

IT has long been known that the extranuclear contributions to radiative capture reactions are appreciable,[1] and several such reactions have been found where these contributions play a dominant role. These reactions are necessarily nonresonant, since they do not follow from the formation of a compound state, and for this reason they have been designated as "direct-capture" reactions. Several examples of direct-capture reactions that have been previously reported are $O^{16}(p,\gamma)F^{17}$,[2] $Ne^{20}(p,\gamma)Na^{21}$,[3] and $D(p,\gamma)He^3$.[4]

The reactions $He^3(\alpha,\gamma)Be^7$ and $T(\alpha,\gamma)Li^7$ are also of the direct-capture type. Calculations by Christy and Duck[5] and by Tombrello and Phillips[6] based on the data of Holmgren and Johnston,[7] have indicated that these experimental results could be understood in a

* Supported by the U. S. Office of Naval Research.
† Present address: Physics Department, Yale University, New Haven, Connecticut.
[1] R. G. Thomas, Phys. Rev. 84, 1061 (1951).
[2] J. B. Warren, K. A. Laurie, D. B. James, and K. L. Erdman, Can. J. Phys. 32, 563 (1954).
[3] N. Tanner, Phys. Rev. 114, 1060 (1959).
[4] G. M. Griffiths and J. B. Warren, Proc. Roy. Soc. (London) A68, 781 (1955).
[5] R. F. Christy and I. Duck, Nucl. Phys. 24, 89 (1961).
[6] T. A. Tombrello and G. C. Phillips, Phys. Rev. 122, 224 (1961).
[7] H. D. Holmgren and R. L. Johnston, Phys. Rev. 113, 1556 (1959).